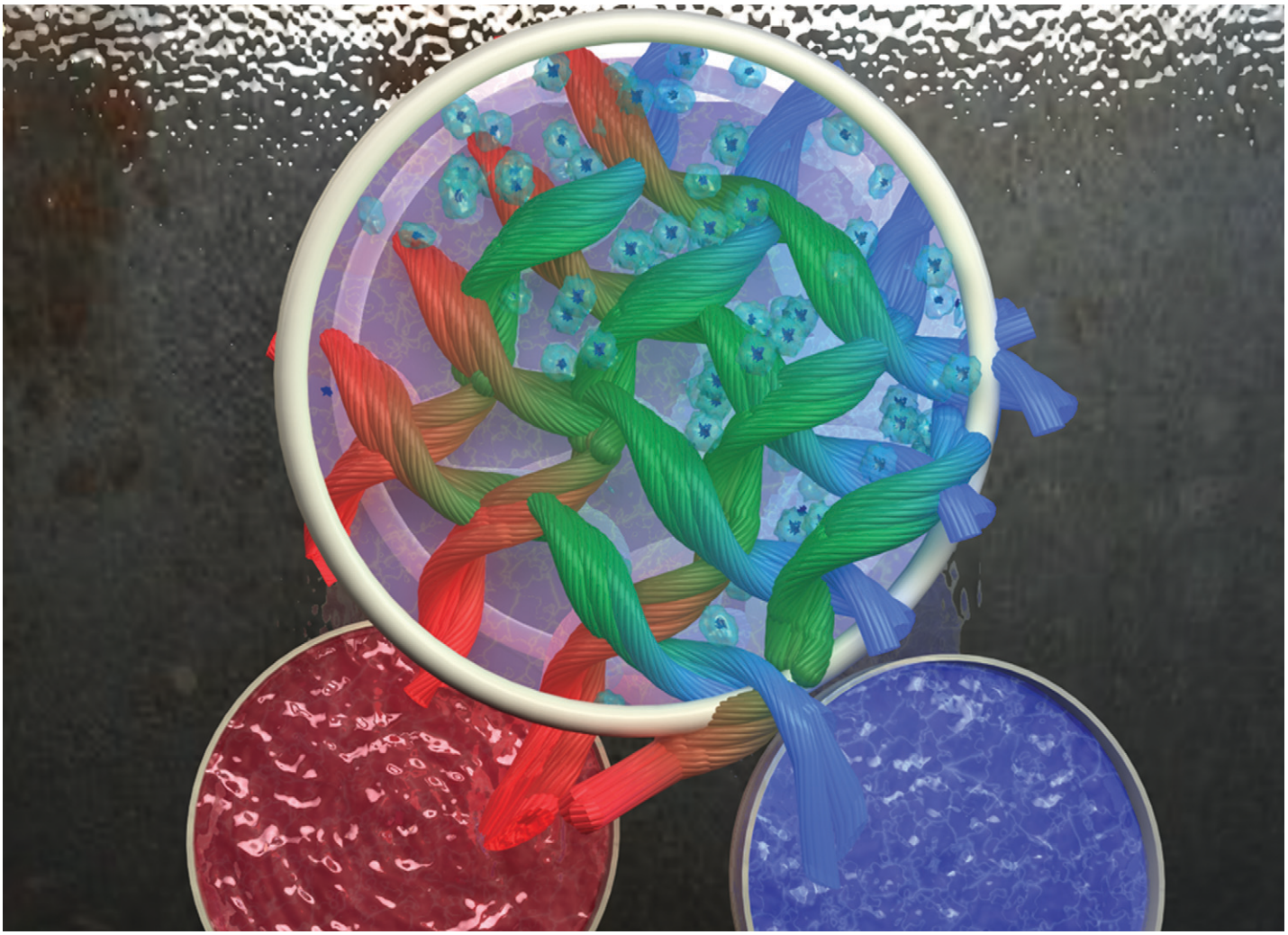

Featuring work from the Micro/Nanophysics Research Laboratory of Professor Leslie Yeo, RMIT University, Australia

Acoustically-driven thread-based tuneable gradient generators

Dynamic spatiotemporal concentration gradients can be stably generated and tuned 'on-the-fly' using sound waves in a thread network embedded within a three-dimensional hydrogel construct to mimic the in vivo tissue microenvironment for microfluidic chemotaxis and cell culture studies.

As featured in:

See Leslie Y. Yeo *et al.*, *Lab Chip*, 2016, **16**, 2820.

ROYAL SOCIETY OF CHEMISTRY

www.rsc.org/loc

Registered charity number: 207890

Lab on a Chip

PAPER

View Article Online
View Journal | View Issue

Cite this: *Lab Chip*, 2016, **16**, 2820

Acoustically-driven thread-based tuneable gradient generators†

Shwathy Ramesan, Amgad R. Rezk, Kai Wei Cheng, Peggy P. Y. Chan and Leslie Y. Yeo*

Received 7th August 2015,
Accepted 12th June 2016

DOI: 10.1039/c5lc00937e

www.rsc.org/loc

Thread-based microfluidics offer a simple, easy to use, low-cost, disposable and biodegradable alternative to conventional microfluidic systems. While it has recently been shown that such thread networks facilitate manipulation of fluid samples including mixing, flow splitting and the formation of concentration gradients, the passive capillary transport of fluid through the thread does not allow for precise control due to the random orientation of cellulose fibres that make up the thread, nor does it permit dynamic manipulation of the flow. Here, we demonstrate the use of high frequency sound waves driven from a chip-scale device that drives rapid, precise and uniform convective transport through the thread network. In particular, we show that it is not only possible to generate a stable and continuous concentration gradient in a serial dilution and recombination network, but also one that can be dynamically tuned, which cannot be achieved solely with passive capillary transport. Additionally, we show a proof-of-concept in which such spatiotemporal gradient generation can be achieved with the entire thread network embedded in a three-dimensional hydrogel construct to more closely mimic the *in vivo* tissue microenvironment in microfluidic chemotaxis studies and cell culture systems, which is then employed to demonstrate the effect of such gradients on the proliferation of cells within the hydrogel.

1 Introduction

Paper-[1–4] as well as thread-based[5–8] microfluidic technology have become increasingly popular of late as point-of-care analytical devices, particularly for use in developing nations where accessibility to healthcare is severely limited.[1,9,10] Both technologies are attractive from the point of view of ease-of-use and low fabrication costs, and hence are amenable as disposable single-use devices which mitigate common risks associated with contamination and disease transmission. Both also rely predominantly on capillary wicking of the sample and reagent through the network as the underlying transport mechanism. Although such passive capillary transport benefits from simplicity both in terms of its setup and operation, it also imposes limits on flow speed, control, directionality, uniformity and reproducibility in paper-based devices, due in particular to the random orientation of the fibres that make up the paper.[11] Additionally, passive capillary transport does not permit flexible and dynamic control. While these limitations may be acceptable in many simple qualitative diagnostic tests, particularly for disease screening in low resource settings at the point of need,[9] there are a number of instances when quantitative or even semi-quantitative analyses are required, in which case the passive capillary flow mechanism becomes inadequate.

There is thus a need to develop better ways to regulate and manipulate the flow through paper and thread networks. For instance, Ballerini *et al.*[12] have demonstrated modular thread sections for switching and mixing in threads whereas modification of a paper's properties, such as its wettability[13] or permeability,[14] have been employed to alter the behaviour of the flow through it. Additionally, both acoustic and electric fields have also exhibited significant potential to modulate and hence regulate transport in paper networks.[11,15] To maintain low cost and simplicity, which constitutes the primary advantages of these devices, creative adaptations to conventional electrode structures have been introduced, for example, using aluminium foil[16] or pencil lead.[15]

Encouraged by the potential of these external fields for flow regulation in *paper*, we show in this work the prospect for rapid and tuneable generation of concentration gradients in *thread* networks and demonstrate the possibility for the entire thread network and its concentration gradient to be embedded within a hydrogel. This is motivated by growing interest in developing microfluidic devices which mimic *in vivo* biomolecular concentration gradients with the aim of facilitating better understanding of the mechanisms that

Micro/Nanophysics Research Laboratory, RMIT University, Melbourne, VIC 3000, Australia. E-mail: leslie.yeo@rmit.edu.au

† Electronic supplementary information (ESI) available. See DOI: 10.1039/c5lc00937e

govern the inter- and intra-cellular signalling cues that regulate a range of biological processes from inflammatory response and axonal regeneration to cancer metastasis and stem cell fate.[17,18] Such understanding could then, in turn, potentially lead to improved design of drugs and therapies.

Since the introduction of the 'Christmas tree' inspired microchannel bifurcation mixer network,[19,20] many strategies for microfluidic gradient generation in microchannel devices have been developed,[21] including those generated *via* acoustic means.[22–24] Most of these, however, are not capable of mimicking the three-dimensional tissue microenvironment—an important factor given that cells in complex three-dimensional tissue have been observed to behave differently from cells grown on two-dimensional tissue culture plates.[25–28] To this end, hydrogels have been employed as three-dimensional extracellular matrix constructs; despite various attempts (see, for example, Haessler *et al.*[29]), however, there remains considerable difficulty in generating concentration gradients within them, at least to similar levels of stability, uniformity and flexibility in spatiotemporal control as that afforded, for example, by two-dimensional microchannel gradient generation devices.

In this work, we therefore attempt to combine the collective advantages of microchannel bifurcation networks for gradient generation, the superior tensile strength of thread compared to paper,[8] the powerful possibility for uniform, stable and dynamic flow regulation facilitated by the use of acoustic fields, and the ability to mimic the *in vivo* local cellular environment using hydrogels. In place of microchannel networks, which would be difficult to embed within the hydrogels, we instead employ a thread lattice interconnected by a series of knots, which has recently been demonstrated as a clever means for splitting and merging, and therefore mixing liquid streams within the thread network.[30] While serial dilution was briefly reported in that work, the reliance on capillary wicking meant that the process was relatively slow and did not allow the possibility for spatiotemporal variation in the gradient, let alone the ability to embed the entire thread network within a hydrogel whilst maintaining a stable gradient.

2 Materials and methods

2.1 Thread network

100% cotton threads (Morris & Sons, Melbourne, VIC, Australia) were employed. Although any porous material that is permeable to the working fluid can be used, in principle, cotton, compared to other thread materials such as rayon and nylon, was primarily used because of its biocompatibility and biodegradability; moreover, it can also be easily degraded using cellulase enzyme. The design of the serial dilution and combinatorial network (Fig. 1(a)), which splits and sequentially recombines two streams was inspired from the design of woven fish nets wherein we use a specialised netting tool (C.H. Smith, Melbourne, VIC, Australia) shown in Fig. 1(b) to produce a serial dilution and recombination network with four generations (Fig. 1(a)). The use of the netting tool as well as

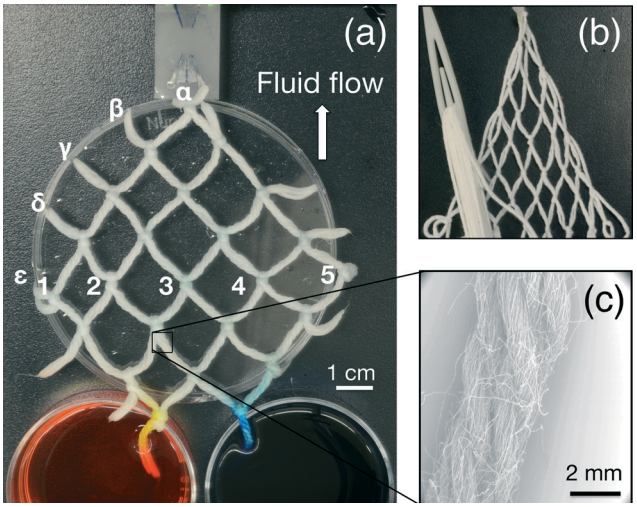

Fig. 1 (a) Thread network connected to the fluid reservoirs and the SAW device, shown here to be placed at a central outlet position α to generate a *symmetric* concentration gradient, although this can successively be moved to different outlet positions β, γ, δ and ε to dynamically tune the gradient 'on the fly' in an *asymmetric* manner. The numeric labels allow identification of the node locations for colourimetric quantification of the mixing. (b) Specialised netting tool used to weave the serial dilution thread network. (c) SEM image of the cotton thread showing the interstitial spaces between the fibres through which fluid is transported.

an embroidery netting technique[31] is important as it allows the formation of identical and precisely-crafted knots, whose topology was shown to control the mixing ratio between two streams flowing into it through the threads that the knot interweaves,[30] in contrast to the hand-made knots in Safavieh *et al.*,[30] which, although simpler, led to run-to-run variations, at least when such knots were attempted in our experiments. Given that Safavieh *et al.*[30] attributed poor predictability and reproducibility due to unequal thread lengths in the different branches in the network, we also took care to ensure equidistance between the knots with the help of a rectangular template of fixed dimension around which the thread was wound. This minimised anomalies in the fluid flow due to variation in the knot distribution; flexibility in the network dimension can then be easily achieved simply by varying the size of the template. A scanning electron microscopy image (SEM; Quanta 200, FEI, Hillsboro, OR, USA) of a thread section is shown in Fig. 1(c) to illustrate the interstitial spaces between the cotton fibres that make up the thread through which the fluid flows. The threads were soaked in deionized water for half an hour to saturate them with liquid prior to the experiments. In contrast to Safavieh *et al.*[30] wherein plasma oxidation of the threads was carried out to improve capillary penetration, the threads were used here without further treatment.

2.2 SAW devices

In a manner similar to that employed in Rezk *et al.*[11] for paper-based devices, we regulate the flow through the thread

network *via* fast and uniform convective transport driven by surface acoustic wave (SAW) nebulisation.[32,33] This was carried out by placing a SAW device, which comprises a 127.86° *Y–X* rotated lithium niobate (LN) single crystal piezoelectric substrate (Roditi Ltd., London, UK) on which interdigitated transducer (IDT) electrodes are photolithographically patterned, at a specific *outlet* position of a particular branch (*e.g.*, α, β, δ, ε or γ in Fig. 1(a)) in the network; it will be shown subsequently that the flow and hence the concentration gradient that is produced can be altered depending on this position. Application of an alternating electrical signal at resonance (in this case, 30 MHz) to the IDTs above a critical input power (typically 2–2.5 W) using a signal generator (SML01, Rhode & Schwarz Pty. Ltd., North Ryde, NSW, Australia) and amplifier (10W1000C, Amplifier Research, Souderton, PA, USA) then leads to nebulisation of the pre-wetted thread at this location, giving rise to a negative pressure that then draws liquid from the inlet reservoir through the thread network *via* a pathway that is dependent on the nebulisation location, *i.e.*, the outlet position where the SAW device is placed (*i.e.*, α, β, δ, ε or γ).

In our setup, the elliptical IDTs consist of forty alternating 33 and 66 nm thick chromium–aluminium finger pairs that produce a focused SAW with a wavelength of 132 μm, corresponding to the 30 MHz resonant frequency. We note that unlike conventional bulk kHz-order ultrasonic nebulisation, the high frequency MHz-order SAW nebulisation does not lead to any considerable biomolecular degradation—this not only allows the SAW to be a powerful tool for microfluidic actuation,[34–36] but also permits the generation of biomolecular concentration gradients in the thread network that facilitates chemotaxis studies for potential drug testing applications.

2.3 Colourimetric quantification

Yellow and blue synthetic food dyes (Queen Fine Foods Pty. Ltd., Alderley, QLD, Australia) prediluted using Milli-Q® water (Merck Millipore Corp., Bayswater, VIC, Australia) were used to visually trace the dynamic mixing of the fluid and hence the generation of the concentration gradient along the network. The extent of mixing between the two dye solutions and hence a quantitative picture of the concentration distribution throughout the thread network, particularly at the knot locations, can then be obtained through a colourimetric analysis based on a hue-saturation-value (HSV) model employed previously (Fig. S1 in the ESI†).[11] An advantage of the HSV method over conventional greyscale pixel intensity analysis is that every colour is associated with a base hue value independent of its intensity or brightness, and as such, the analysis is insensitive to variations in the illumination conditions between experimental runs.[11] The hue values vary correspondingly as the colour changes with the progressive mixing of the dyes at locations along the thread network, which can then be tracked both in space and time.

Briefly, high resolution time-lapse images were acquired using a digital SLR camera (D600, Nikon Corp., Shinjuku, Japan). The hue values at each knot location H, calculated by averaging the individual hue value of each pixel spanning the knot area, which can be extracted from the images using MATLAB®(Mathworks Inc., Natick, MA), then allows us to obtain a percentage blue intensity value at each knot location:

$$\%\text{blue} = \left(\frac{H_{\text{yellow}} - H}{H_{\text{yellow}} - H_{\text{blue}}} \right) \times 100. \quad (1)$$

$H_{\text{yellow}} \approx 50$ and $H_{\text{blue}} \approx 210$ are the hue values of yellow and blue, respectively, such that equimixing of both solutions gives a green solution with a hue value of $H_{\text{green}} \approx 130$. To avoid nonuniform mixing of the colours, we employ equal dye volumes in the blue and yellow solution reservoirs from which the threads at the inlet of the network draw.

2.4 Hydrogel synthesis

To show that the concentration gradient can be generated and stably sustained in addition to being dynamically tuned within an extracellular matrix, thus constituting a superior mimic of the cell response in a three-dimensional tissue microenvironment, we carry out a demonstrative experiment in which we embed the entire thread network in a hydrogel. Here, we employ a 5% gelatin-hydroxyphenyl propionic acid (Gtn-HPA) hydrogel synthesized using a general carbodiimide/active ester-mediated oxidative coupling reaction of the phenol moieties in distilled water;[37–41] the enzymatic reaction allowing independent tuning of the hydrogel stiffness and the gelation rate. In brief, 5 g gelatin (Gtn, M_w = 80–140 kDa; Wako Pure Chemical Industries Ltd., Osaka, Japan) and 0.864 g 3,4-hydroxyphenylpropionic acid (HPA; Sigma-Aldrich Pty. Ltd., Castle Hill, NSW, Australia) was first dissolved in 250 mL Milli-Q® water. To this solution, 0.573 g *N*-hydroxysuccinimide (NHS; Sigma-Aldrich Pty. Ltd., Castle Hill, NSW, Australia) and 0.955 g 1-ethyl-3-(3-dimethylaminopropyl)-carbodiimide hydrochloride (Sigma-Aldrich Pty. Ltd., Castle Hill, NSW, Australia) was added. The mixture was stirred overnight at room temperature at a constant pH of 4.7, followed by further dialysis against NaCl, 25% ethanol, and water in the aforementioned sequence for 2 days each to remove toxic unconjugated substances. The final product was then lyophilised in 50 ml falcon tubes for 2 days until the water content was completely removed. The precursor that forms has a spongy structure and is stable at room temperature. Conjugation of Gtn to HPA was further confirmed by ^{1}H NMR (D_2O) analysis. Detection of chemical shifts at 6.8 and 7.2 ppm indicated the presence of aromatic protons in the combination. Cross-linking to form the hydrogel was initiated by adding 100 units per mg horseradish peroxidase (HRP; Wako Pure Chemical Industries Ltd., Osaka, Japan) and diluted 30% H_2O_2 (Sigma-Aldrich Pty. Ltd., Castle Hill, NSW, Australia). The HRP concentration is optimised in this work such that the gelation occurred precisely at a predetermined time period, in this case 19 seconds, when the thread network was gently placed within the hydrogel to

be embedded. A circular Petri-dish was used to mould the hydrogel constructed, which was subsequently extruded out to form a free standing substrate that is 1.3 cm thick and 2.5 cm in radius.

2.5 Cell culture and characterisation

Human fibrosarcoma (HT1080) cells were acquired from the American Type Culture Collection (ATCC, Rockville, MD) and maintained in Dulbecco's Modified Eagle Medium (DMEM-GIBCO) supplemented with 10% fetal bovine serum and 1% penicillin–streptomycin. The cells were subcultured periodically every 2–3 days and passaged at no more than 90% confluency. The incubator was constantly maintained at 37 °C with 95% relative humidity and 5% CO_2. All cell culture media and supplements as well as chemicals employed for the characterisation of the cells described below were purchased from Life Technologies Pty. Ltd. (Mulgrave, VIC, Australia) unless specified otherwise.

Discs made from the hydrogels synthesised using the method in section 2.4 were first fabricated.[41] Briefly, 5% Gtn-HPA solution (5 mg mL^{-1} in PBS) was sterilised *via* filtration through 0.22 μm syringe filters under aseptic conditions and centrifuged to obtain a bubble free solution to which 5 μL of HRP was added to yield a final concentration of 0.13 units per mL. Crosslinking was then initiated by adding 10 μL of H_2O_2 solution to give final concentrations of 3.2 mM, before adding to a standard 35 mm Corning® dish. The prefabricated cotton network was gently plunged into the dish halfway through gelation to embed the cotton network into the gelating solution. The gels were subsequently allowed to set for an hour at room temperature following by uniform seeding of the HT1080 cells over their surface at a density of 3750 cells per mm^2. The cells were allowed to adhere in complete media for 24 hours and the growth medium removed prior to exposure to the gradients of complete media and 1× phosphate buffered saline (PBS), generated and stabilised in the thread network *via* SAW excitation.

The viability of the cells within the Gtn-HPA hydrogel constructs were assessed at different time points using calcein acetoxymethyl (AM) and propidium iodide (PI). Prior to staining, the hydrogel constructs were first washed twice with PBS; staining with calcein AM (2 μM) and PI (4 μM) took place over 45 min at 37 °C in the absence of exposure to light. The hydrogels were then washed twice with PBS to remove excess dye and the fluorescent images of the cells at different nodes of the thread network were captured at 20× magnification (ZOE™ Fluorescent Cell Imager, Bio-Rad Laboratories Inc., Hercules, CA).

To determine the number of cells inside the hydrogel at each time point, we uniformly extract a small 3 mm^2 circular area of a separate hydrogel construct around each nodal position labelled 1 through 5 in Fig. 1(a) and place this in a 96-well plate. The hydrogel construct was then digested in 200 μL 0.25% trypsin–EDTA solutions by incubating the hydrogels at 37 °C for 2 hours. The cells released from the degraded hydrogels were subsequently collected and stained with 0.4% trypan blue solution. Since non-viable cells assume a blue colouration of the solution and viable cells remain unstained, the total number of live and dead cells can then be enumerated using a haemocytometer.

To assess the cellular metabolic activity and hence their proliferation at different time points, the 3 mm^2 circular hydrogel constructs were extracted using the aforementioned method and placed in a 96-well plate. 200 μL of 3-(4,5-dimethylthiazolyl-2)-2,5-diphenyltetrazolium bromide (MTT) solution (1 mg mL^{-1} in serum free medium) was added to each well and the cells were further incubated at 37 °C for 6 h. The reduction of MTT by the metabolically active cells due to the dehydrogenase enzyme results in the formation of purple formazan crystals that is then imaged under bright-field illumination at 20× magnification (ZOE™ Imager, Bio-Rad Laboratories Inc., Hercules, CA). After removal of the unreacted MTT solution from the wells, the crystals can also be solubilised by incubation in 200 μL of dimethyl sulfoxide (DMSO) over 30 min, and subsequently quantified *via* absorbance measurements of the solution at 570 nm (Spectramax® Paradigm multimode plate reader, Molecular Devices LLC, Sunnyvale, CA).

Finally, the morphology and F-actin arrangement of the cells were visualised through cytoskeleton (actin) and nuclear (DAPI) staining. Briefly, the aforementioned extracted hydrogel constructs were fixed in 4% paraformaldehyde at room temperature for 1.5 hours. The hydrogels were then washed twice with sterile PBS before adding 1% BSA for 30 minutes at room temperature to avoid nonspecific staining. After further washing twice with PBS, the hydrogels were individually stained with DAPI (2 μg mL^{-1} in PBS) and Alexa Fluor 488® phalloidin (5 μM mL^{-1} in PBS) for 1.5 hours. Excess dye was washed with PBS and the cells were imaged using laser scanning confocal microscopy (Eclipse Ti, Nikon Instruments Inc., Melville, NY) with 495 nm (green; actin) and 340 nm (blue; DAPI) excitation filters.

3 Results and discussion

The initial experiments were carried out in the absence of the hydrogel to characterise and optimise the concentration gradient in the thread network. Fig. 2(a) shows the formation of a continuous symmetric concentration gradient in the serial dilution thread network as the yellow and blue solutions are drawn from their respective reservoirs through the network towards the outlet location α (see Fig. 1(b)) where the SAW device is located when it is activated and nebulisation ensues. As the coloured solutions progressively mix, it can be seen that a stable symmetric gradient throughout the network is formed—all within 10 minutes, which is considerably faster compared to the case of passive capillary action in the absence of the SAW excitation wherein a similar gradient forms over a duration of 45 minutes (Fig. 2(b)). The increase in speed can be attributed to the convective transport generated by the SAW which *pulls* fluid through the thread network at constant speed (*i.e.*, the position of the advancing

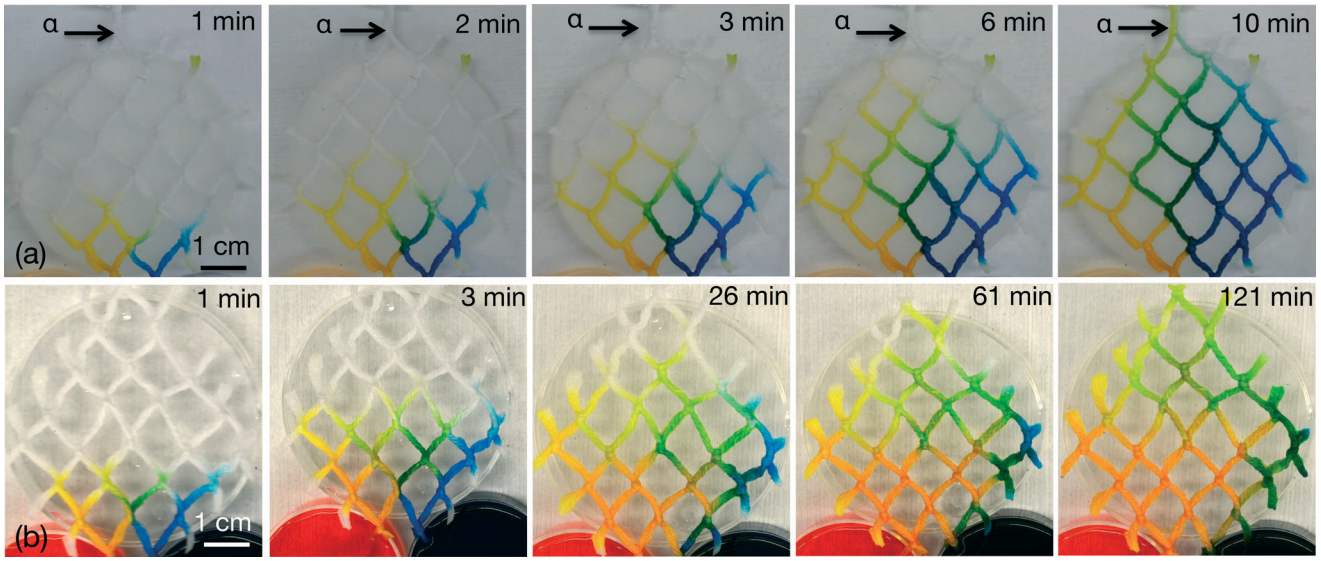

Fig. 2 (a) Time series images showing the transport and mixing of two coloured solutions, yellow and blue, through the serial dilution and combinatorial thread network, drawn from the reservoirs at the bottom of the images (one inlet thread port was immersed in each reservoir) towards the outlet at location α when the SAW device placed at this location is activated. Due to the serial dilution and mixing, a stable symmetric concentration gradient across the network can be seen. (b) Corresponding time series image showing the transport and mixing similar to (a) but in the absence of the SAW device such that the flow of the dye solutions through the thread is driven solely by capillarity. Not only does it take significantly longer for the dyes to penetrate the thread network, the mixing appears non-uniform and is hard to reproduce.

liquid front x through the thread scales linearly with time t)[11] as opposed to passive capillary diffusive transport wherein the fluid is *pushed* through the thread network at a speed that follows the Washburn $x \sim t^{1/2}$ scaling.[12,42] A benefit of the faster convective transport afforded by the SAW is that the reduced times lead to a lower propensity for loss of sample or the thread drying out due to evaporation. We note that the knots at the network junctions where the threads twist and overlap also aid in the mixing[30] in a similar way that the stretching and folding of laminar streams lead to enhanced mass transport as a result of the increase in interfacial area and a reduction in striation thicknesses,[43] although the gradient generated through passive capillary transport in the absence of the SAW did not appear to be as uniform, as seen in Fig. 2(b), or reproducible.

In addition to faster formation of the concentration gradient, a further advantage with the use of the SAW to drive fluid transport through the thread network is the ability to dynamically alter and hence tune the concentration gradient 'on the fly'—which is not possible with passive capillary transport—thus offering the possibility of mimicking real biological or physiological processes which are essentially dynamical in nature.[44,45] This is done simply by switching the outlet position at which the SAW device is placed from one branch to another (*e.g.*, locations β, δ, ε and γ in Fig. 1(a)) while keeping the input power and frequency to the device

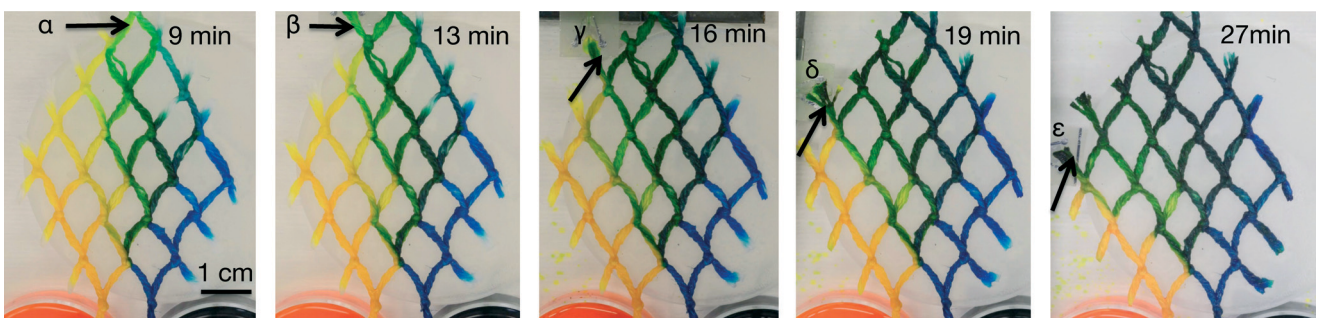

Fig. 3 Time series images showing the dynamic tuning of the concentration gradient in the serial dilution thread network. Initially, the SAW device was placed at outlet position α to generate a symmetric concentration gradient shown in the first image at 9 minutes wherein the ratio of blue to yellow colouration in the network is close to 50% due to equal mixing of the dyes. Progressively shifting the SAW device away from the central position at α to positions β, γ, δ and ε subsequently increases the asymmetry in the concentration gradient, as shown by the successive images from left to right, as less of the yellow dye is pulled through the network, preferring the shortest route through the thread to the outlet where the SAW device is placed. The arrow shown in the images indicates the position of the SAW device.

constant to maintain a stable nebulisation rate. As seen in Fig. 3, the concentration gradient becomes increasingly asymmetric as the position of the SAW device is sequentially moved further away from the central outlet position α, resulting in less of the yellow solution penetrating the majority of the network, preferring instead the path of least resistance through the shortest route toward the outlet where the SAW device is located. If the SAW device were to be shifted to the other outlet positions on the side of the blue reservoir, a mirror symmetric result in the asymmetric concentration gradient that is formed is obtained in which less of the blue solution penetrates the network. In the experiment, we allow several minutes between the switching to enable the concentration gradient to stabilise and equilibrate. An alternative to the above setup in which a single SAW device is manually repositioned at the different outlet positions is the use of several SAW devices, one at each outlet location of every branch, and simply switching the nebulisation from one to the other.

Following Safavieh *et al.*,[30] we model the mixing ratios in the serial dilution thread network by exploiting the analogy between the fluidic resistance in the thread with that in electrical circuits. As the knots act as resistors and the net flux into and out of the knot is zero, it is then possible to apply Kirchoff's junction rule at each knot to predict the relative concentration ratios between the blue and yellow solutions. Fig. 4 shows the predictions of the mixing ratio, represented as a percentage of the blue dye concentration, from this simple network theory at the different node locations in the thread network (see Fig. 1(a)) when the SAW device is placed at the different outlet positions, confirming our earlier observation that a concentration gradient exists such that the concentration of blue dye decreases laterally across the network (*i.e.*, moving laterally across from node 1 to node 5 in Fig. 1(a) wherein node 1 is the node location on the farthest side of the blue reservoir) regardless of the position of the SAW device. Clearly, and again in agreement with our earlier observations on the dynamic tuneability of the concentration gradient, moving the SAW device closer to the yellow reservoir from position β to ε leads to an increase in the blue concentration across nodes 1 to 5 (in other words, less of the yellow solution penetrates the network). The inset in Fig. 4, on the other hand, shows the average percentage error between the theoretical prediction and the experimental data, indicating decent agreement with errors typically below 10% although we note that the error grows with increasing asymmetry in the gradient when the SAW device is located at the extremities (*i.e.*, location ε). This is due to the shorter flow path from inlet to outlet as the location of the SAW device is moved further away from the central outlet position α, thus resulting in weaker cross-flow through the orthogonal branches, which unfortunately is not captured by the theory which assumes equal flow in the branches that are both parallel and orthogonal to the main flow branch.

It is possible to embed the entire serial dilution thread network within a hydrogel whilst maintaining a continuous

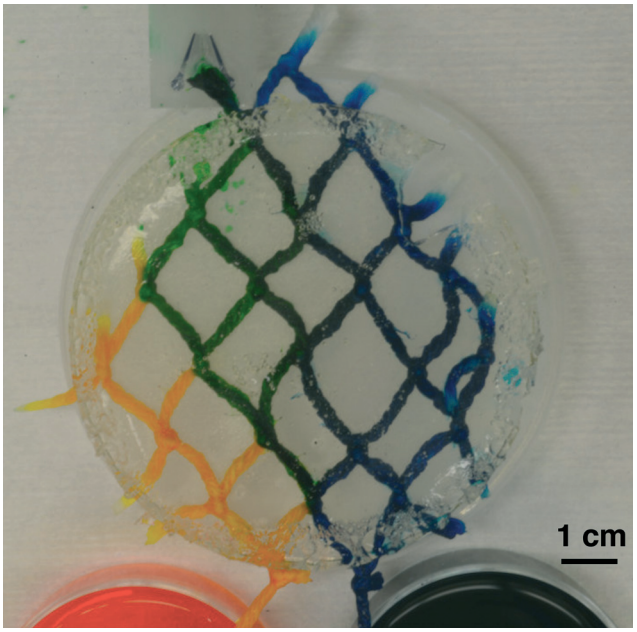

Fig. 5 Image showing the serial dilution thread network embedded in a transparent Gtn-HPA hydrogel (without cells) of 2.5 cm radius and 1.3 cm thickness as it crosslinks. Once the thread network is embedded, the SAW was used to generate the concentration gradient in the same way that is done in the absence of a hydrogel, thus verifying as a proof-of-concept that a stable concentration gradient can be generated and maintained within the hydrogel in a controlled manner. Some microbubbles are observed at the edges of the round hydrogel construct due to active vortexing of the crosslinkers and the polymer precursor.

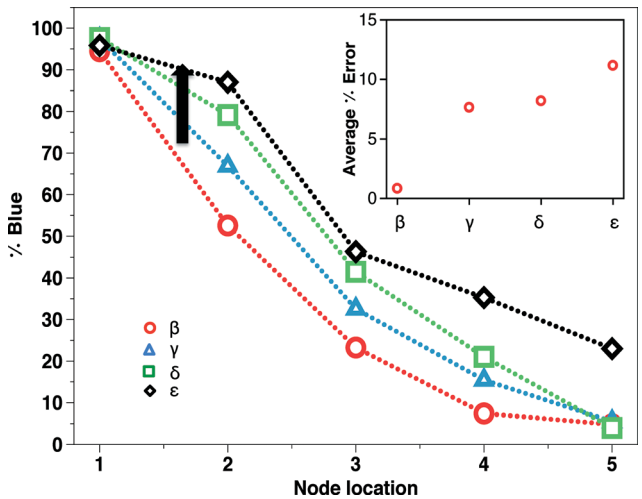

Fig. 4 Mixing ratio represented by the percentage of the blue dye concentration as predicted by the simple network theory at the node locations shown in Fig. 1(a) (node 1 represents the node location on the farthest side of the blue reservoir and node 5 on the farthest side of the yellow reservoir) for the different SAW device positions β to ε as it is moved closer to the yellow reservoir. The arrow indicates the trend in which the percentage of blue dye across the network increases as the SAW device is moved in this manner as less of the yellow dye penetrates the network. The trendlines were added to guide visualisation. The inset shows the percentage error between the theoretical and experimental values averaged across the nodal positions on a particular branch for each case when the SAW device location is moved.

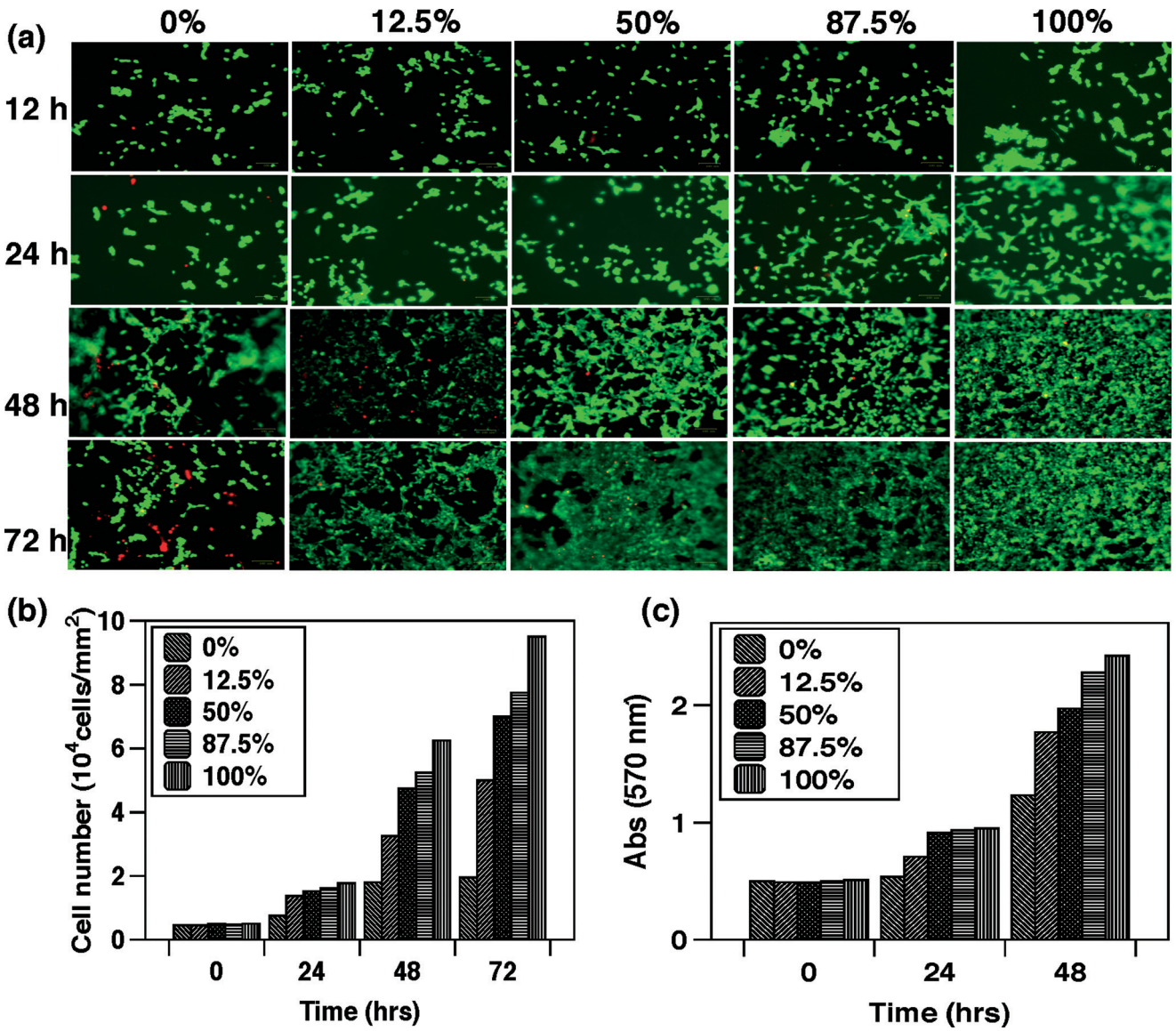

Fig. 6 Viability and proliferation of cells in the Gtn-HPA hydrogel construct at different time points after exposure to the SAW stabilised nutrient gradient in the thread network. (a) Representative images showing fluorescent live/dead staining of the cells at different node locations in the thread network (positions 1 to 5 in Fig. 1(a)) corresponding to DMEM : PBS ratios of 0, 12.5%, 50%, 87.5% and 100%, respectively, at 12, 24, 48 and 72 hours after exposure to the SAW stabilised nutrient gradient in the thread; green cells stained by calcein AM represent viable cells whereas red cells stained by PI represent those that are dead. Each panel represents an area of the hydrogel disc construct that is approximately 1 mm × 750 μm. (b) Total cell count using the trypan blue assay at various time points at nodal positions 1 to 5, which correspond to the different nutrient concentration ratios. (c) Absorbance reading corresponding to the cell metabolic activity and hence its proliferation ability at different time points and node locations across the thread network, as measured *via* the MTT assay.

and stable concentration gradient that can still be dynamically tuned, as indicated in the proof-of-concept (shown without cells for the purposes of clarity in imaging the gradient) in Fig. 5. We note some slight distortion in the shape of the network due to contractile forces that cause the hydrogel to shrink as it crosslinks, although this does not appear to influence the quality of the concentration gradient generated in the network. This ability to not only create but to also maintain a stable concentration gradient within a tissue construct is an important step towards carrying out microfluidic chemotaxis studies that more closely mimics the *in vivo* three-dimensional tissue microenvironment, hence allowing a better understanding of biological and physiological processes such as cell signalling and migration, wound healing and angiogenesis, among others. Moreover, the ability to tune the concentration gradient within the hydrogel 'on-the-fly', which is not possible with passive capillary transport, represents a significant step forward in offering the ability to dynamically regulate and alter the microenvironment during the cell culture or chemotaxis study. This is aided further by the ability

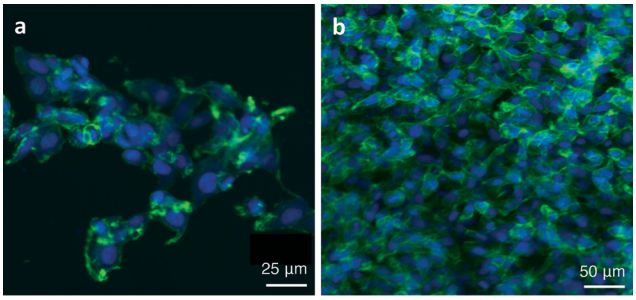

Fig. 7 Confocal microscopy images of the extracted hydrogel constructed in a (a) nutrient-poor environment (0% medium concentration) at nodal location 1 (see Fig. 1(a)), and, (b) nutrient-rich environment (100% medium concentration) at nodal location 5. The cell nuclei stained by DAPI is shown in blue whereas cell F-actin networks stained by phalloidin are displayed in green.

to tune the stiffness of the hydrogel with the H_2O_2 concentration or even its porosity with the addition of porogens or *via* enzymatic degradation.[40,41,46]

Fig. 6 shows the proliferation of HT1080 cells seeded in the hydrogel construct when they are exposed to nutrient gradients (DMEM and PBS) in the thread network, as a simple example of its utility to mimic three-dimensional tissue microenvironments. Given that it is well established that cell viability and proliferation depends critically on nutrient supply in the growth medium,[47,48] a corresponding gradient in the cell viability—demonstrated through the green fluorescent stain of the live/dead assay in Fig. 6(a) and quantified *via* the enumeration of viable *vs.* nonviable cells with the trypan blue assay in Fig. 6(b), and its proliferation capability—captured through results of the MTT assay in Fig. 6(c) and Fig. S2 in the ESI,† can be seen across the thread network and becomes increasingly prominent in time (cells located in the immediate vicinity of each of the node locations 1 through 5 in the thread network as shown in Fig. 1(a), corresponding to a DMEM : PBS ratios of 0, 12.5%, 50%, 87.5% and 100%, respectively, were assessed at different time points, *i.e.*, 12, 24, 48 and 72 hours of exposure to the gradient stabilised by the SAW). In stark contrast, the control experiments in the absence of SAW excitation such that no concentration gradient exists in the thread network showed no significant difference in the cell viability and proliferation characteristics across the same node locations (Fig. S3 in the ESI†).

As further confirmation of the effect of the SAW generated gradient on cell survival and proliferation in the thread network, it is also possible to observe the morphological changes to the cells. Fig. 7 shows confocal microscopy images of the cells after 72 hours of exposure to 0% and 100% medium concentration (corresponding to nodal locations 1 and 5 in Fig. 1(a), respectively) in the thread network. Not only are there fewer cells in the nutrient-poor environment (Fig. 7(a)), cells starved of nutrients also exhibit poorly organised F-actin structure that are predominantly spherical or ellipsoidal. In contrast, cells in the nutrient-rich environment (Fig. 7(b)) are seen to be more abundant, growing confluently and displaying highly elongated F-actin and clearly defined stress fibres.

4 Conclusion

In this work, we combine the concept of a microfluidic serial dilutor in the form of a thread-based lattice network interconnected by a series of knots using a netting technique together with acoustically-driven convective flow transport using high frequency MHz order sound waves that permits rapid, precise and uniform flow control in porous materials. This is exploited for the generation of stable continuous concentration gradients in the thread network with speeds much faster and with more uniformity and reproducibility in the mixing than that which can be achieved *via* passive capillary transport. More importantly, we demonstrate the possibility of dynamically tuning the concentration gradient in the thread network simply by shifting the acoustomicrofludic device to another outlet position on a different branch of the network—a capability that cannot be achieved with pure capillary flow through the thread. Finally, we show that this operation can be carried out with the entire thread-based concentration generation network embedded in a cell-laden three-dimensional hydrogel construct whose material properties can also be tuned, therefore providing a superior mimic of an *in vivo* tissue microenvironment for chemotaxis and cell culture compared to a conventional two-dimensional microchannel-based concentration gradient generator.

5 Acknowledgements

ARR is grateful for a Vice-Chancellor's Postdoctoral Fellowship from RMIT University. LYY is the recipient of a Future Fellowship (FT130100672) from the Australian Research Council (ARC), who also funded part of the work through Discovery Project grant DP140100805.

References

1 A. W. Martinez, S. T. Phillips, Z. Nie, C.-M. Cheng, E. Carrilho, B. J. Wiley and G. M. Whitesides, *Lab Chip*, 2010, **10**, 2499–2504.
2 X. Li, D. R. Ballerini and W. Shen, *Biomicrofluidics*, 2012, **6**, 011301.
3 A. K. Yetisen, M. S. Akram and C. R. Lowe, *Lab Chip*, 2013, **13**, 2210–2251.
4 D. M. Cate, J. A. Adkins, J. Mettakoonpitak and C. S. Henry, *Anal. Chem.*, 2015, **87**, 19–41.
5 M. Reches, K. A. Mirica, R. Dasgupta, M. D. Dickey, M. J. Butte and G. M. Whitesides, *ACS Appl. Mater. Interfaces*, 2010, **2**, 1722–1728.
6 X. Li, J. Tian and W. Shen, *ACS Appl. Mater. Interfaces*, 2010, **2**, 1–6.
7 G. Zhou, X. Mao and D. Juncker, *Anal. Chem.*, 2012, **84**, 7736–7743.
8 A. Nilghaz, D. Ballerini and W. Shen, *Biomicrofluidics*, 2013, **7**, 051501.

9 P. Yager, T. Edwards, E. Fu, K. Helton, K. Nelson, M. Tam and B. Weigl, *Nature*, 2006, **442**, 412–418.
10 P. Yager, G. J. Domingo and J. Gerdes, *Annu. Rev. Biomed. Eng.*, 2008, **10**, 107–144.
11 A. R. Rezk, A. Qi, J. R. Friend, W. H. Li and L. Y. Yeo, *Lab Chip*, 2012, **12**, 773–779.
12 D. R. Ballerini, X. Li and W. Shen, *Biomicrofluidics*, 2011, **5**, 014105.
13 H. Noh and S. T. Phillips, *Anal. Chem.*, 2010, **82**, 4181–4187.
14 I. Jang and S. Song, *Lab Chip*, 2015, **15**, 3405–3412.
15 P. Mandal, R. Dey and S. Chakraborty, *Lab Chip*, 2012, **12**, 4026–4028.
16 A. R. Rezk, J. R. Friend and L. Y. Yeo, *Lab Chip*, 2014, **14**, 1802–1805.
17 T. M. Keenan and A. Folch, *Lab Chip*, 2008, **8**, 34–57.
18 S. Kim, H. J. Kimz and N. L. Jeon, *Integr. Biol.*, 2010, **2**, 584–603.
19 S. K. W. Dertinger, D. T. Chiu, N. L. Jeon and G. M. Whitesides, *Anal. Chem.*, 2001, **73**, 1240–1246.
20 N. L. Jeon, H. Baskaran, S. K. W. Dertinger, G. M. Whitesides, L. V. D. Water and M. Toner, *Nat. Biotechnol.*, 2002, **20**, 826–830.
21 A. G. G. Toh, Z. P. Wang, C. Yang and N.-T. Nguyen, *Microfluid. Nanofluid.*, 2014, **16**, 1–18.
22 D. Ahmed, C. Y. Chan, S.-C. S. Lin, H. S. Muddana, N. Nama, S. J. Benkovic and T. Jun Huang, *Lab Chip*, 2013, **13**, 328–331.
23 G. Destgeer, S. Im, B. Hang Ha, J. Ho Jung, M. Ahmad Ansari and H. Jin Sung, *Appl. Phys. Lett.*, 2014, **104**, 023506.
24 P.-H. Huang, C. Y. Chan, P. Li, N. Nama, Y. Xie, C.-H. Wei, Y. Chen, D. Ahmed and T. J. Huang, *Lab Chip*, 2015, **15**, 4166–4176.
25 P. D. Benya and J. D. Shaffer, *Cell*, 1982, **30**, 215–224.
26 S. J. Bryant and K. S. Anseth, *J. Biomed. Mater. Res.*, 2002, **59**, 63–72.
27 A. Abbott, *Nature*, 2003, **424**, 870–872.
28 D. R. Albrecht, G. H. Underhill, T. B. Wassermann, R. L. Sah and S. N. Bhatia, *Nat. Methods*, 2006, **3**, 369–375.
29 U. Haessler, M. Pisano, M. Wu and M. A. Swartz, *Proc. Natl. Acad. Sci. U. S. A.*, 2011, **108**, 5614–5619.
30 R. Safavieh, G. Z. Zhou and D. Juncker, *Lab Chip*, 2011, **11**, 2618–2624.
31 P. Blandford, *Netmaking*, Brown, Son & Ferguson, Glasgow, 4th edn, 1969.
32 A. Qi, L. Yeo, J. Friend and J. Ho, *Lab Chip*, 2010, **10**, 470–476.
33 L. Y. Yeo and J. R. Friend, *Annu. Rev. Fluid Mech.*, 2014, **46**, 379–406.
34 J. Friend and L. Yeo, *Rev. Mod. Phys.*, 2011, **83**, 647–704.
35 S.-C. S. Lin, X. Mao and T. J. Huang, *Lab Chip*, 2012, **12**, 2766.
36 X. Ding, P. Li, S.-C. S. Lin, Z. S. Stratton, N. Nama, F. Guo, D. Slotcavage, X. Mao, J. Shi, F. Costanzo and T. J. Huang, *Lab Chip*, 2013, **13**, 3626–3649.
37 M. Kurisawa, F. Lee, L.-S. Wang and J. E. Chung, *J. Mater. Chem.*, 2010, **20**, 5371–5375.
38 S. P. Hoo, Q. L. Loh, Z. Yue, J. Fu, T. T. Tan, C. Choong and P. P. Chan, *J. Mater. Chem. B*, 2013, **1**, 3107–3117.
39 A. Al-Abboodi, J. Fu, P. M. Doran and P. P. Chan, *Biotechnol. Bioeng.*, 2013, **110**, 318–326.
40 A. Al-Abboodi, J. Fu, P. M. Doran, T. T. Tan and P. P. Chan, *Adv. Healthcare Mater.*, 2014, **3**, 725–736.
41 A. Al-Abboodi, R. Tjeung, P. M. Doran, L. Y. Yeo, J. Friend and P. P. Chan, *Adv. Healthcare Mater.*, 2014, **3**, 1655–1670.
42 E. W. Washburn, *Phys. Rev.*, 1921, **17**, 273–283.
43 J. M. Ottino, *Annu. Rev. Fluid Mech.*, 1990, **22**, 207–254.
44 P. Zheng, B. He and W. Tong, *et al.*, *Neurol. India*, 2014, **62**, 280.
45 D. De Silva, K. Kunasegaran, S. Ghosh and A. M. Pietersen, *BMC Dev. Biol.*, 2015, **15**, 7.
46 L.-S. Wang, J. Boulaire, P. P. Chan, J. E. Chung and M. Kurisawa, *Biomaterials*, 2010, **31**, 8608–8616.
47 N. M. Moore, N. J. Lin, N. D. Gallant and M. L. Becker, *Acta Biomater.*, 2011, **7**, 2091–2100.
48 U. Riekstina, R. Muceniece, I. Cakstina, I. Muiznieks and J. Ancans, *Cytotechnology*, 2008, **58**, 153–162.